



RESEARCH ARTICLE

Synchrotron micro-scale study of trace metal transport and distribution in *Spartina alterniflora* root system in Yangtze River intertidal zone

Huan Feng¹ · Weiguo Zhang² · Wenliang Liu² · Lizhong Yu² · Yu Qian^{1,5} · Jun Wang³ · Jia-Jun Wang³ · Christopher Eng³ · Chang-Jun Liu⁴ · Keith W. Jones⁴ · Ryan Tappero³

Received: 11 February 2015 / Accepted: 13 July 2015 / Published online: 26 July 2015
© Springer-Verlag Berlin Heidelberg 2015

Abstract This study is focused on micro-scale measurement of metal (Ca, Cl, Fe, K, Mn, Cu, Pb, and Zn) distributions in *Spartina alterniflora* root system. The root samples were collected in the Yangtze River intertidal zone in July 2013. Synchrotron X-ray fluorescence (XRF), computed microtomography (CMT), and X-ray absorption near-edge structure (XANES) techniques, which provide micro-meter scale analytical resolution, were applied to this study. Although it was found that the metals of interest were distributed in both epidermis and vascular tissue with the varying concentrations, the results showed that Fe plaque was mainly distributed in the root epidermis. Other metals (e.g., Cu, Mn, Pb, and Zn) were correlated with Fe in the epidermis possibly

due to scavenge by Fe plaque. Relatively high metal concentrations were observed in the root hair tip. This micro-scale investigation provides insights of understanding the metal uptake and spatial distribution as well as the function of Fe plaque governing metal transport in the root system.

Keywords *Spartina alterniflora* · Trace metals · Synchrotron radiation technique · Rhizosphere root system · Transport · Yangtze River estuary

Responsible editor: Elena Maestri

Highlight

- Synchrotron radiation measurement is applied to micro-scale investigation.
- Expression of metal uptake, transport, and distribution varies with metals.
- Fe plaque is found in the epidermis and can scavenge other metals.
- Factors controlling metal uptake and translocation are evaluated

✉ Huan Feng
fengh@mail.montclair.edu

- ¹ Department of Earth and Environmental Studies, Montclair State University, Montclair, NJ 07043, USA
- ² State Key Laboratory of Estuarine and Coastal Research, East China Normal University, Shanghai 200062, People's Republic of China
- ³ Photon Sciences Directorate, Brookhaven National Laboratory, Upton, NY 11973, USA
- ⁴ Biological, Environmental & Climate Sciences Department, Brookhaven National Laboratory, Upton, NY 11973, USA
- ⁵ Present address: School of Ecology and Environmental Sciences, Yunnan University, Kunming, Yunnan 650091, People's Republic of China

Introduction

Previous studies have shown that wetland plants can uptake heavy metals from rhizosphere soils and sediments through the root system and store these metals within the plant biomass (Williams et al. 1994; Lacerda et al. 1997; Tangahu et al. 2011; Koelmel and Amarasiriwardena 2012). Significant correlations between metal concentrations in plants and the surrounding soils were also found (Cheng 2003; Weis and Weis 2004; Rotkittikhum et al. 2006; Qian et al. 2012; Lyubenova et al. 2013). However, very limited high resolution information is available on metal uptake, distribution, and transport processes in the plants. In the meantime, the function of Fe plaque that is predominantly Fe oxides in metal uptake by the plants is still not well understood despite Fe plaque has been identified as a buffer or barrier capable of enhancing or reducing plant metal uptake efficiency in many studies (Tripathi et al. 2014). Some studies suggest that the Fe plaque on the root surface serves as a barrier preventing metals from entering plant roots (e.g., St-Cyr and Campbell 1996; Sundby et al. 1998), while others argue that Fe plaque is not the main barrier (e.g., Ye et al. 1998; Liu et al. 2004). More information is needed to make broad inferences in this aspect. Therefore, investigation of the natural processes that control the metal translocation in

wetland plants is critical to understand metal biogeochemical cycle. *Spartina alterniflora*, which takes up and accumulates metals during its growth (Windham et al. 2003), is a dominant wetland species in the Yangtze River intertidal zone. Because of its geographical location next to one of the world's largest urban areas and within one of the world's largest estuarine systems, the wetland in Yangtze River intertidal zone is a unique test bed for examination of metal uptake by wetland plants. The synchrotron-based techniques with high detection sensitivity and analytical resolution for elemental composition measurement have been employed by the environmental science community (Jones and Feng 2002; Sutton et al. 2002; Punshon et al. 2009; Jones et al. 2013). In this study, synchrotron radiation techniques are applied to investigate metal transport and distributions in *S. alterniflora* root as well as the function of Fe plaque in metal scavenge in the root system. This research certainly improves our current knowledge of metal distributions and transport in the wetland plants.

Materials and methods

Study area

The Yangtze River estuary, which is one of the largest estuaries in the world, is defined as a mesotidal estuary with a mean tidal range of 2.6 m and a mean spring tidal range of 4.0 m. Under the fair weather conditions, the Yangtze River estuary is dominantly influenced by tides that affect the estuarine water circulation and sediment deposition. The channel on the north side of Chongming Island, where the study site is located, is flood tide dominated, while the channel on the south side of Chongming Island is ebb tide dominated. There is evidence showing that there exists lateral residual circulation in the estuary, making water and sediment exchanges between the channels in the estuary (e.g., Wu et al. 2010). Huge amount of sediments ($\sim 4.86 \times 10^8$ ton year⁻¹) have been discharged from the Yangtze River annually, resulting in an extensive intertidal zone in the Yangtze River estuary (Chen 1998). This well-developed intertidal zone typically contains three distinct vegetation units seaward: a *Phragmites australis* zone, a *Scirpus mariqueter* zone, and *Scirpus triqueter* zone and bare unvegetated mudflats (Zhang et al. 2001). In the late 1990s, *S. alterniflora* was planted on Jiuduansha Shoal as well as the eastern end of Chongming Island for promotion of sediment accretion and coastal defense. It is now becoming a predominant species in the area. Urbanization and economic development in Shanghai, which is the largest city in China and located next to the Yangtze River estuary, have a direct impact on the Yangtze River estuary. Industrial and domestic sewage is discharged into the Yangtze River estuary (Dai and Gu 1990). In addition to the local waste discharge, many land areas in or adjacent to the intertidal zone are used for

commercial harbors, iron and steel mills, and other industrial operations (Chen et al. 2007). Previous studies have shown that environmental quality in the Yangtze River estuary has been degraded due to urbanization and industrial development in Shanghai metropolitan area (Feng et al. 2004; Liu et al. 2006; Zhang et al. 2009).

Sample collection and preparation

S. alterniflora replicate samples were collected in the Yangtze River intertidal zone (31° 35' 4.95" N, 121° 54' 15.43" E) in July 2013 (Fig. 1). After the collection, the samples were placed in a large plastic container and then transported immediately to East China Normal University in Shanghai for further laboratory treatment. Bulk sediments on the roots were removed by hand. The trace residual sediments on the roots were rinsed off gently with a small amount (<20 ml) of deionized water. Some of the fresh root samples were processed immediately for analysis. The others were oven dried separately at 30 °C and archived for future analysis. For synchrotron computed microtomography (CMT) analysis, a dried clean section of 2-cm-long root sample was put in a Kapton tube ($\Phi < 1$ mm), sealed on both ends, and put on a stand for the analysis (Jones et al. 2013). The cleaned fresh root samples for synchrotron X-ray fluorescence (XRF) measurement were suspended in an optimal cutting temperature (OCT) compound that does not infiltrate the specimen, and cooled at -20 °C. Once OCT solidified, a cryotome (Cryostat

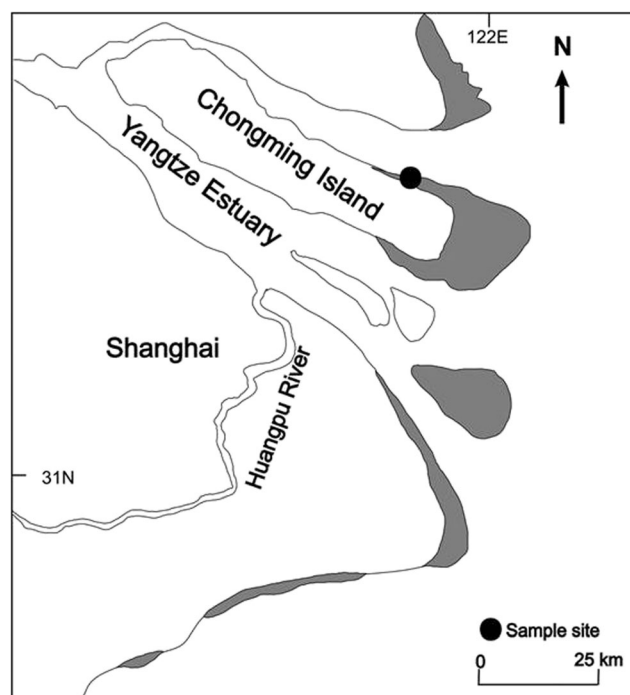


Fig. 1 Map showing the sampling site on the north shore of Chongming Island in the Yangtze River intertidal zone

CM1950, Leica Microsystems) was used to cut a 50- μm -thin section and then mounted on a 25 mm \times 76 mm quartz microscope slide (SPI Supplies[®]) (Feng et al. 2013). For synchrotron X-ray absorption near-edge structure (XANES) measurement, a portion (~1 mm in length) of dry root samples was sectioned and mounted on a needle stand for the analysis. Before the analysis, all these samples were kept in our specially designed biology laboratory with a temperature control at 4 °C or a desiccator.

Synchrotron X-ray CMT, XRF, and XANES measurement

Synchrotron CMT measurement was made at X2B beamline in the National Synchrotron Light Source (NSLS) at Brookhaven National Laboratory (BNL) in Upton, New York, USA (Jones et al. 2005, 2013). The tomography apparatus uses a Si (1, 1, 1) monochromator to produce a monoenergetic beam of 10.0 keV. A beam size of about 6 mm \times 6 mm was used to irradiate the root sample contained in the Kapton tube. The beam transmitted through the sample was detected with a CsI (Tl) scintillator. The light from the scintillator was magnified and then imaged with a CCD camera with 1340 \times 1300 pixels of 4 μm in size. The tomographic volume was produced from a collection of 1200 images taken in 0.15° steps. The volume was produced using the tomo_display software (<http://cars.uchicago.edu/software/IDL/tomography.html>). The analysis and visualization was achieved with the ImageJ package (<http://imagej.nih.gov/ij/>). Elemental (Ca, Cl, Cu, Fe, K, Mn, Pb, and Zn) concentrations and distributions in the root tissue were investigated using synchrotron XRF technique at NSLS X27A beamline (Ablett et al. 2006; Feng et al. 2013). Briefly, this bend magnet beamline uses Kirkpatrick-Baez (K-B) mirrors to produce a focused spot (10 μm \times 10 μm) of hard X-rays with tunable energy achieved via Si(111) or Si(311) channel-cut monochromator

crystals. For synchrotron XRF imaging, the incident beam energy was fixed at 13.5 keV to excite all target elements simultaneously. The sample was oriented at 45° to the incident beam and rastered in the path of the beam by an XY stage, while X-ray fluorescence was detected using a 13-element Canberra Ge array detector positioned at 90° to the incident beam. Elemental maps were typically collected from a 1 mm² sample area using a step size of 15 μm and a dwell time of 7 s. The fluorescence yields were normalized to the changes in intensity of the X-ray beam (I_0) and the dwell time. Synchrotron XANES measurement was conducted at NSLS X8C beamline that was equipped with a full-field transmission X-ray microscope (TXM) manufactured by Xradia, Inc. (Wang et al. 2012; Jones et al. 2013). The newly developed TXM provides a large field of view (40 μm \times 40 μm), 30-nm resolution, local tomography, and automated maker-free image acquisition and alignment (Wang et al. 2012, 2014a). By tuning X-ray energy across the absorption edge of the element of interesting, this TXM technique enables chemical information with high sensitivity (Wang et al. 2014b). In order to investigate Fe distribution in the roots, the XANES data were collected by scanning the X-ray energy from 7092 to 7192 eV with a step size of 2 eV in this study. A stack of images was obtained by scanning the photon energy across the X-ray absorption edge of elemental Fe. A lens-coupled scintillator with a 2048 \times 2048 pixel camera detector was used to record images. With all 1024 \times 1024 pixels for bin 2 \times 2, the full spectrum for each pixel was extracted. The XANES analysis was carried out using a customized program (MatLab, MathWorks, R2011b) developed in house (beamline X8C group, NSLS, BNL). Background normalization was carried out first for TXM images with a unique background image collected at every energy. More information about TXM and XANES can be found in Wang et al. (2013, 2014b). A tomographic dataset was collected using 361 projections at a range between -90°

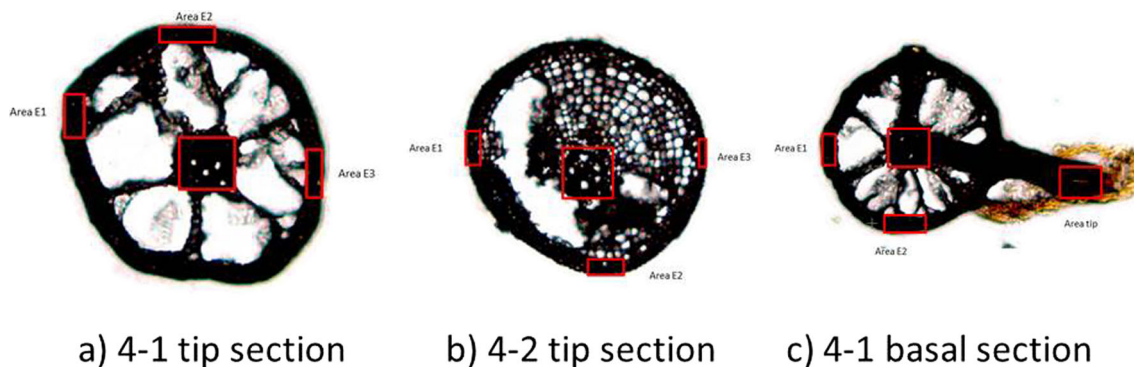


Fig. 2 Optical images showing the structure of *Spartina alterniflora* root cross sections: **a** 4-1 tip section, **b** 4-2 tip section, and **c** 4-1 basal section. Roots 4-1 and 4-2 are replicate samples. The thickness of the cross sections is 50 μm . These thin cross section samples are prepared for

synchrotron XRF measurement for metal concentrations and distributions. The areas framed in the root epidermis, vascular tissue, and hair tip are extracted for data analysis

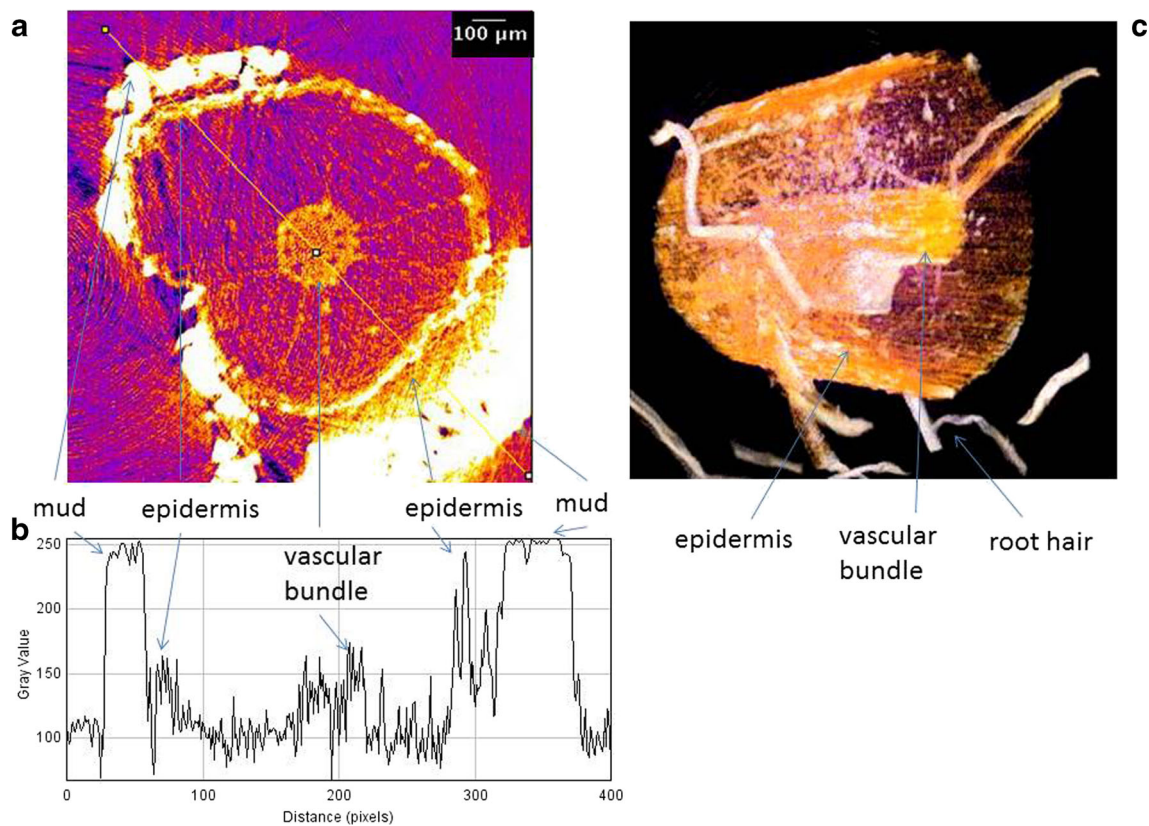


Fig. 3 Two- and three-dimensional reconstructed images of synchrotron X-ray computed microtomography (CMT) measurement on *Spartina alterniflora* root: *a* two-dimensional image of *S. alterniflora* root cross

section, *b* profile of attenuation along the cross section labeled in the two-dimensional image, and *c* three-dimensional image of *S. alterniflora* root with root hair showing

and $+90^\circ$ (2×2 camera pixels with 10-s exposure time). The reconstruction and visualization of the experimental data were accomplished using proprietary software developed by Xradia, Inc.

Data extraction for statistical analysis

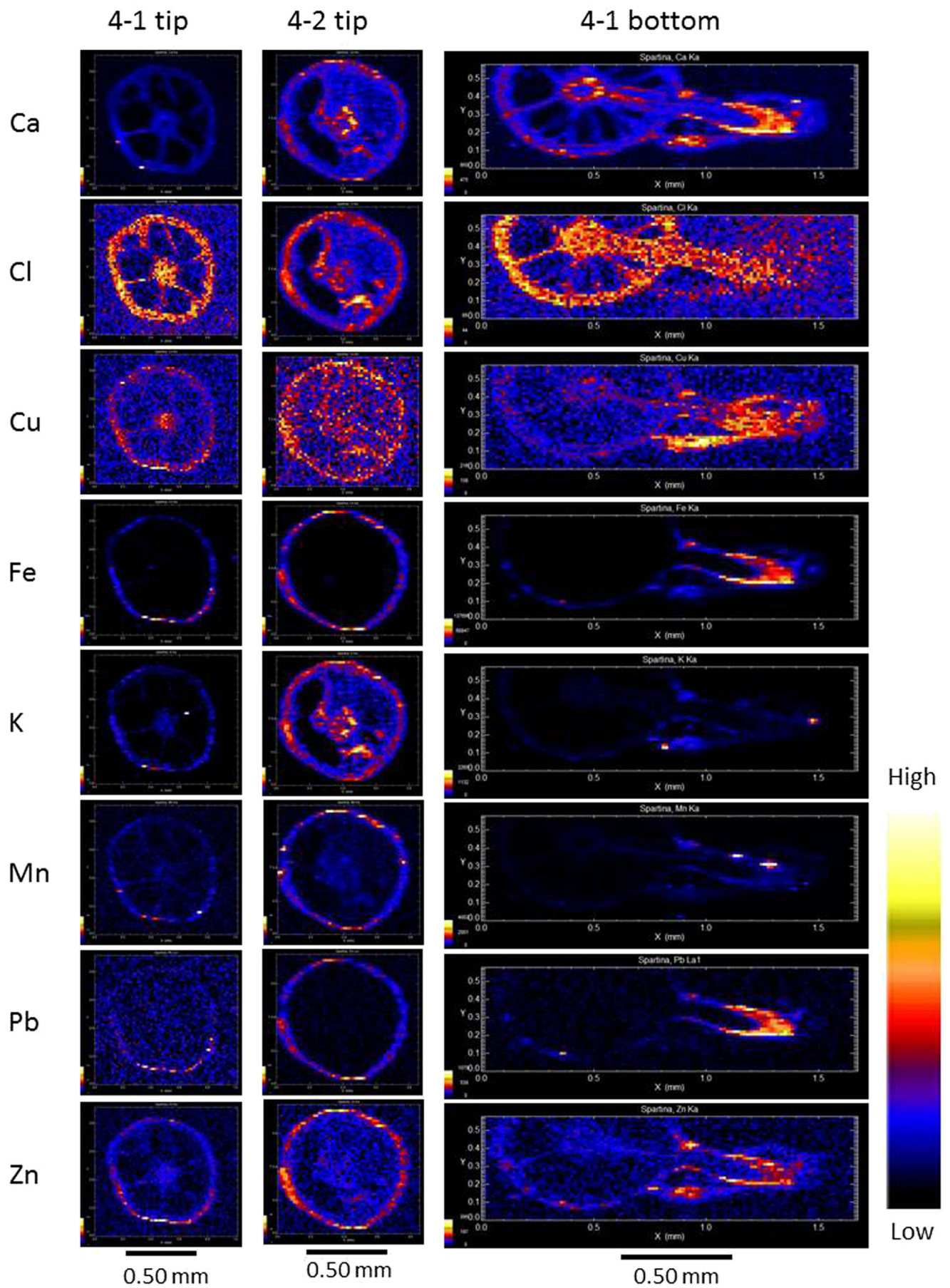
In order to investigate factors governing the metal transport and accumulation and to avoid excessive data processing, we selected two to three sub-areas in the epidermis and one broad sub-area in the vascular tissue within the plant root section (Fig. 2a, b) as well as one area in the root hair tip (Fig. 2c). Data acquisition was made from two-dimensional scan or mapping, and data in sub-areas were extracted and used for the statistical analysis. Each sub-area in the epidermis contained 30 to 90 points measured for metal concentrations. There were a total of 484 points in the epidermis among the three samples, which were used for statistical analysis. In the vascular bundle, each sub-area contained 110 to 130 points measured for the metal concentrations. There were a total of 372 points selected in the vascular tissue among the three samples for statistical analysis. The sub-area in the root hair tip section contained 152 points for statistical analysis. Each

sub-area in the root tissue showed a range of metal concentrations.

Statistical analysis

Student's *t* test analysis was performed on the data to examine metal concentration differences between epidermis and vascular tissue of each plant root. Factor analysis and hierarchical cluster analysis were also performed on the data. Logarithmic transformation of the data was made before the analysis to ensure a normal distribution (Gotelli and Ellison 2004). In factor analysis, varimax rotation was applied to maximize the sum of the variance of the factor coefficients. In hierarchical clustering analysis, single linkage method (nearest neighbor) and Pearson correlation (distance) were applied in the analysis.

Fig. 4 Metal concentrations and distributions in *Spartina alterniflora* root cross sections. Sections 4-1 tip and 4-2 tip are replicates of the root tip samples from two *S. alterniflora* root samples. Sections 4-1 tip and 4-1 bottom are the tip and basal sections of the same root sample. The extension in the 4-1 bottom section is the root hair



Results

Micro-scale tomographic root structure and metal concentrations in the root tissue

Three-dimensional visualization of tomographic *S. alterniflora* root structure is shown in Fig. 3. High attenuation substances are seen in the epidermis. Although the chemical composition of the high-attenuation substance cannot be identified in this study using the current synchrotron CMT measurement, synchrotron XRF measurement confirms that Cl, Ca, K, Fe, Mn, Cu, Pb, and Zn are concentrated within these substances. Figure 4 shows these metal concentrations and distributions in the root cross section from the epidermis to the vascular tissue. It is seen that Fe and Pb have relatively much higher concentrations in the epidermis than in the vascular tissue, forming a nearly continuous, surficial rind on the root exterior (Fig. 4). Among the other elements (Ca, Cl, K, Mn, Cu, and Zn), which are essential nutrients for the plant growth, Cl, Mn, and Zn show relatively higher concentrations in the epidermis than in the vascular tissue, while Ca shows relatively higher concentration in the vascular tissue than in the epidermis (Fig. 4). The concentrations of Cu and K in the epidermis and vascular tissue are comparable (Fig. 4). It is interestingly observed that very high metal concentrations are present in the root hair tip (Fig. 4). It is well known that the function of root hairs is to take up water and mineral nutrients present in the sediments and transport these nutrients through the roots to the rest of the plant (McLaughlin et al. 1998; Hinsinger and Courchesne 2008; Marques et al. 2009).

Table 1 summarizes the range and average of element/metal concentrations in all the selected sub-areas within the epidermis, vascular tissue, and root hair tip. In general, Cl, Fe, Mn, Pb, and Zn have higher average concentrations in the epidermis than in the vascular tissue while Ca has higher average concentration in the vascular tissue than in the epidermis. Average concentrations of Cu and K are comparable between the epidermis and vascular tissue. Except Cl and K, metals have higher average concentrations in the root hair tip than in the main root (Table 1).

Statistical analysis

To examine the differences in metal concentrations between the epidermis and the vascular tissue and between the root and the root hair tip in the cross section of the same sample, Student's *t* test was performed on the data. Significant differences ($p < 0.01$) were found in all the cases except for Cu ($p = 0.372$) and K ($p = 0.098$) between the epidermis and the vascular tissue. The results suggest that the uptake mechanisms by plants and transport pathways within the plant tissues could be different for different metals. In addition, both factor analysis and hierarchical cluster analysis were applied to the data analysis (Gotelli and Ellison 2004). In the factor analysis, the root tissues were divided into three groups (epidermis, vascular tissue, and root hair tip) and analyzed separately. As shown in Table 2, four factors in the epidermis with eigenvalue greater than 0.5 account for 86 % of the total variance. Factor 1 has high loadings of Ca (0.865) and moderate loadings of Zn (0.680), Mn (0.561), and Fe (0.495) and explains 24 % of

Table 1 Metal concentrations (cps) in different tissue parts of *Spartina alterniflora* root system. Data are extracted from the selected sub-areas in the epidermis, vascular tissue and hair tip

Element	Statistics	Epidermis (n=484)	Vascular tissue (n=372)	Hair tip (n=152)
Ca	Mean±S.D.	181±76	248±100	387±185
	Range	24–560	45–825	105–833
Cl	Mean±S.D.	75±54	65±43	31±12
	Range	0–276	9–203	4–58
Cu	Mean±S.D.	38±17	40±18	85±24
	Range	0–106	0–99	0–184
Fe	Mean±S.D.	6139±10,290	157±324	41,649±30,182
	Range	60–74,279	31–3605	1136–120,691
K	Mean±S.D.	81±73	89±79	69±43
	Range	0–336	0–526	0–284
Mn	Mean±S.D.	80±86	59±27	795±3530
	Range	0–674	0–159	37–35,082
Pb	Mean±S.D.	85±134	19±17	368±249
	Range	0–1050	0–66	0–946
Zn	Mean±S.D.	63±42	48±22	115±63
	Range	0–292	0–122	5–347

Table 2 Results of factor analysis. The threshold of eigenvalue is set at 0.5

	Eigenvalue=0.5						
	Rotated loading matrix (varimax, gamma=1.000000)						
	1	2	3	4	5	6	7
Epidermis							
log ₁₀ Ca	0.865	0.207	0.218	0.136			
log ₁₀ Zn	0.680	0.110	0.084	0.457			
log ₁₀ Mn	0.561	0.274	0.018	0.600			
log ₁₀ Cl	0.093	0.893	0.002	0.272			
log ₁₀ K	0.271	0.882	0.032	0.179			
log ₁₀ Cu	0.172	0.013	0.980	0.066			
log ₁₀ Pb	0.150	0.227	0.070	0.905			
log ₁₀ Fe	0.495	0.322	0.056	0.732			
Variance explained by rotated components	1.904	1.861	1.025	2.052			
Percent of total variance explained	23.804	23.263	12.811	25.653			
Vascular tissue							
log ₁₀ Cl	0.931	-0.116	0.021	0.189	-0.01	0.006	0.056
log ₁₀ K	0.917	-0.051	-0.025	0.013	-0.032	0.195	0.178
log ₁₀ Cu	-0.13	0.979	0.089	-0.064	0.085	0.062	-0.033
log ₁₀ Pb	-0.001	0.085	0.994	0.044	0.027	-0.04	-0.014
log ₁₀ Fe	0.155	-0.065	0.047	0.97	0.006	0.052	0.149
log ₁₀ Zn	-0.03	0.081	0.027	0.005	0.994	0.053	-0.009
log ₁₀ Ca	0.139	0.065	-0.043	0.052	0.058	0.967	0.174
log ₁₀ Mn	0.187	-0.035	-0.015	0.159	-0.01	0.184	0.95
Variance explained by rotated components	1.805	0.998	1.002	1.011	1.001	1.018	0.992
Percent of total variance explained	22.565	12.48	12.529	12.64	12.516	12.72	12.394
Root hair tip							
log ₁₀ Fe	0.962	-0.124	0.005				
log ₁₀ Ca	0.952	0.014	-0.056				
log ₁₀ Pb	0.923	-0.163	0.027				
log ₁₀ Zn	0.918	0.061	0.008				
log ₁₀ Mn	0.763	0.282	0.097				
log ₁₀ K	0.742	0.246	0.088				
log ₁₀ Cu	0.032	0.956	-0.109				
log ₁₀ Cl	-0.035	0.1	-0.989				
Variance explained by rotated components	4.662	1.11	1.01				
Percent of total variance explained	58.27	13.878	12.631				

the variance (Table 2). This factor is a Ca factor and reflects the association of these metals (Ca, Fe, Mn, and Zn) as nutrients in the epidermis. Factor 2 has high loadings of Cl (0.893) and K (0.882) and accounts for 23 % of the variance. Although both Cl and K are nutrients for the plants, they are also major elements in seawater. This factor may reflect salt tolerance on *S. alterniflora*. As a salt marsh species, *S. alterniflora* can uptake Cl and K in seawater and, hence, grow up in estuarine system. Factor 3, which has a high loading of Cu (0.980), is essentially a Cu-controlling factor and accounts

for 13 % of the total variance. Factor 4 has high loadings of Pb (0.905) and Fe (0.732) and moderate loadings of Mn (0.600) and Zn (0.457) and explains 26 % of the total variance. This factor reflects metal (Pb, Mn, and Zn) scavenging by or adsorption on Fe plaque and co-precipitation of Pb and Zn with Fe-Mn oxides. In the vascular tissue, there are seven factors which have an eigenvalue greater than 0.5 and account for 98 % of the total variance (Table 2). Factor 1 has high loadings of K (0.931) and Cl (0.917) and explains 23 % of the total variance. This factor also reflects sea salt influence on

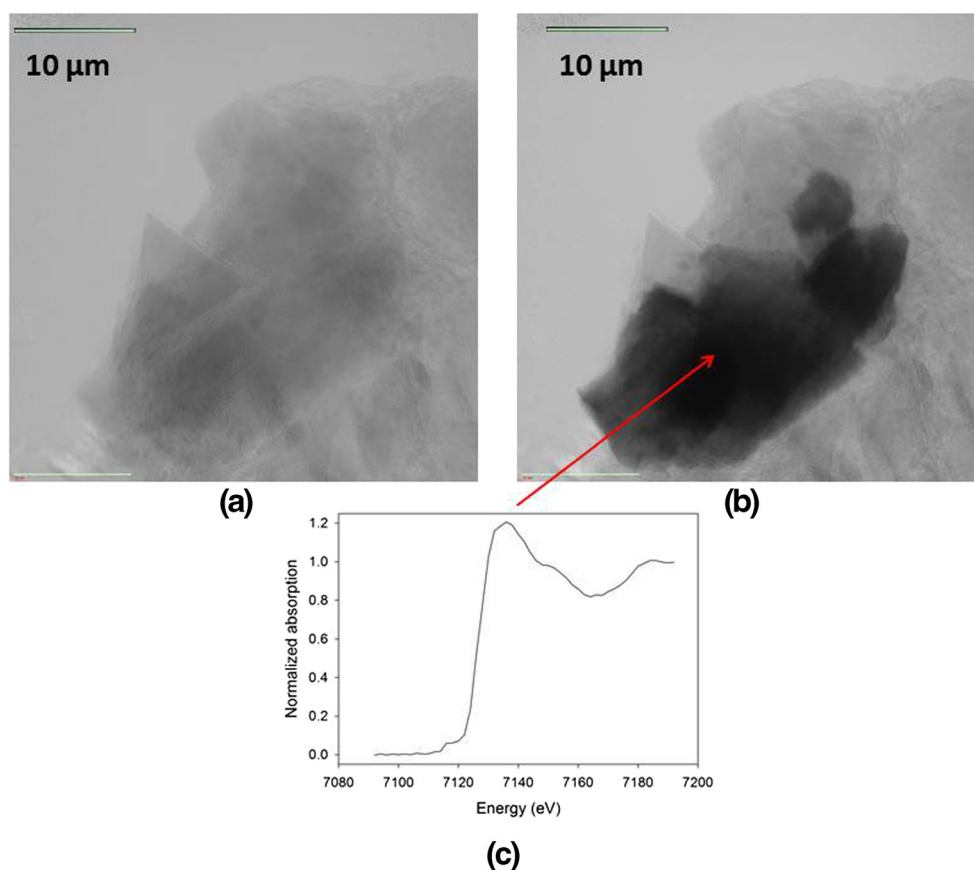
saltwater *S. alterniflora* in the estuarine system. Factors 2–7 have high loadings of Cu (0.979), Pb (0.994), Fe (0.970), Zn (0.994), Ca (0.967), and Mn (0.950), respectively, and almost equally explain the total variance (12–13 %) (Table 2). These factors are essentially individual factors of Cu, Pb, Fe, Zn, Ca, and Mn and control the transport and distribution of these metals in the vascular tissue. In the root hair tip section, there are three factors with an eigenvalue greater than 0.5. They explain 85 % of the total variance. Factor 1 has high loadings of Fe (0.962), Ca (0.952), Pb (0.923), Zn (0.918), Mn (0.763), and K (0.742) (Table 2). It explains 58 % of the total variance and reflects the uptake of metals as nutrients and the function of Fe plaque in metal scavenge. Factors 2 and 3 have high loadings of Cu (0.956) and Cl (–0.989) and explain 14 and 13 % of the total variance, respectively (Table 2). These two factors are individual factors specifically for Cu and Cl uptake and transport. In the hierarchical clustering analysis (Gotelli and Ellison 2004), the root tissue was analyzed separately for the epidermis, vascular tissue, and root hair tip. The data treatment was the same as that performed in the factor analysis. Elements used for the cluster analysis were Ca, Cl, Cu, Fe, K, Mn, Pb, and Zn. Figure 7a shows three clusters formed in the epidermis. K and Cl form one cluster. Fe and Mn, which are then joined in sequence by Pb, Zn, and Ca, form another cluster. Cu is independent of other parameters and stays alone.

Both K and Cl are major ions in seawater and components of salt. Therefore, these two elements cluster together. Fe and Mn form Fe-Mn oxides that can co-precipitate or scavenge other trace metals such as Pb and Zn. Ca is a major required nutrient for plants. Although Cu is also a nutrient for the plant growth, the result suggests that the expression of uptake and transport process of Cu may be different from other trace metals. In the vascular tissue, K and Cl form a cluster and then are joined in sequence by Mn, Ca, Fe, and Zn (Fig. 7b). Pb and Cu loosely form another cluster (Fig. 7b). In the root hair tip, Fe and Ca cluster together closely and then are joined in sequence by Pb, Zn, Mn, and K (Fig. 7c). In the meantime, Cu and Cl loosely cluster together (Fig. 7c).

Discussions

Previous studies have shown that rhizosphere in wetlands is a favorable environment for microbial communities (Emerson et al. 1999; Frenzel et al. 1999; Gilbert and Frenzel 1998; King and Garey 1999; Liu et al. 2004; Perret et al. 2000; Wang and Peverly 1999). In the rhizosphere, biogeochemical reactions, such as metal oxidation and complexation, most likely occur at the interface between plant roots and rhizosphere soils/sediments. It is understandable that metal concentrations in the

Fig. 5 Synchrotron X-ray absorption near-edge structure (XANES) measurement confirms the spatial distribution of Fe plaque in the epidermis of *Spartina alterniflora* root: *a* Fe XANES image taken at 7092 eV (below Fe²⁺ pre-edge), *b* Fe XANES image taken at 7192 eV (above Fe³⁺ pre-edge), and *c* Fe XANES spectrum of a point in the center of Fe plaque as indicated by an *arrow*. The shadows in *a*, where Fe plaque was found, indicate the absorption of other metals, such as Mn, Cu, and Ni, whose pre-edges are below Fe pre-edge. The results suggest the metal scavenge by Fe plaque or Fe-Mn oxides



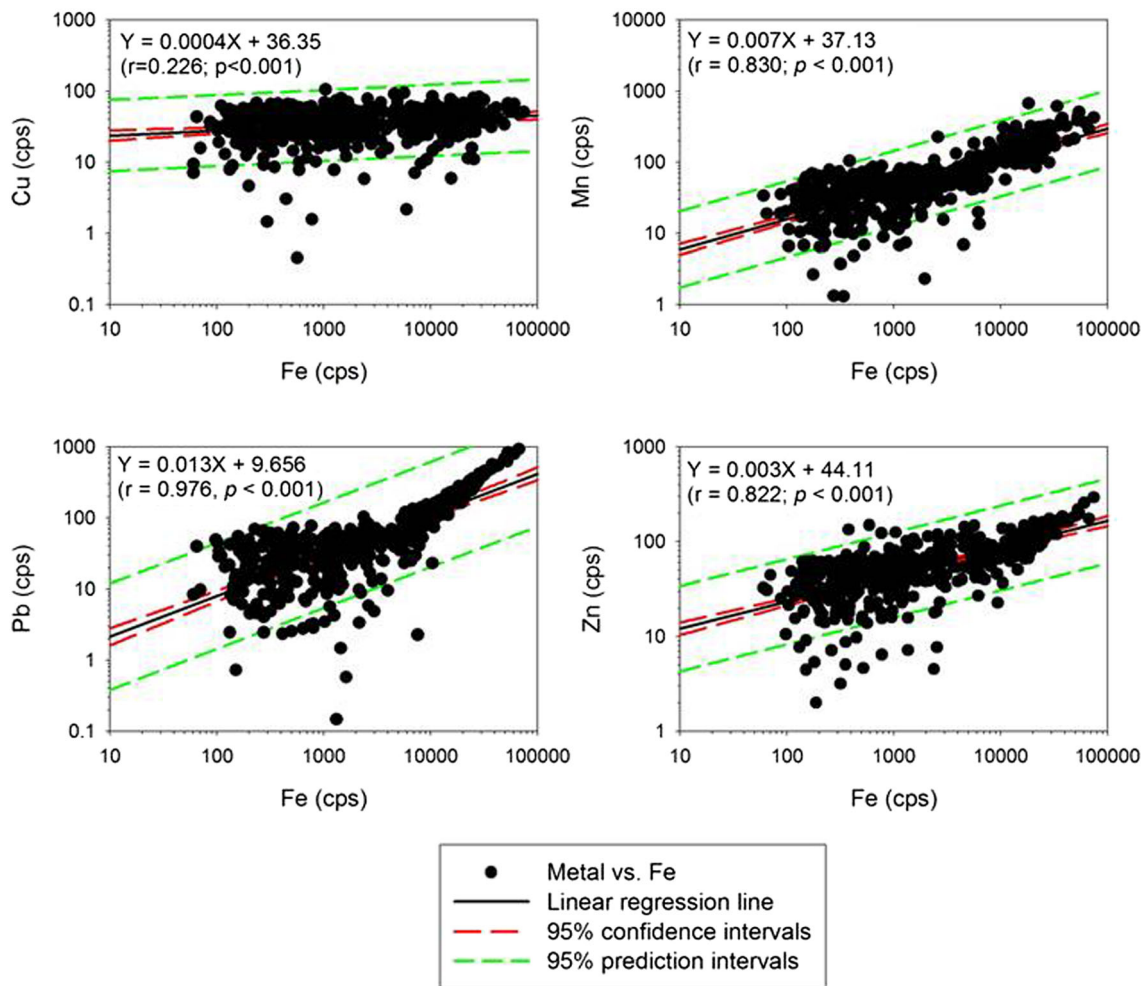


Fig. 6 Significant correlations ($p<0.001$) of Cu, Mn, Pb, and Zn with Fe in all the sub-areas within the epidermis of *Spartina alterniflora* roots

sediments and plant tissue are usually very different because metals in the sediments are from natural weathering processes (Loring 1991; Taylor and McLennan 1995) or anthropogenic input (Feng et al. 1998; Zhang et al. 2009) while metals in the plant tissues are due to plant uptake, translocation, and

bioconcentration (Gleason et al. 2003; Martin et al. 2006; Qian et al. 2012). Nevertheless, the nutrients required for the plant growth are acquired from the rhizosphere sediments. Due to its large-specific surface area, root hair makes absorbing both water and mineral nutrients more efficient. In

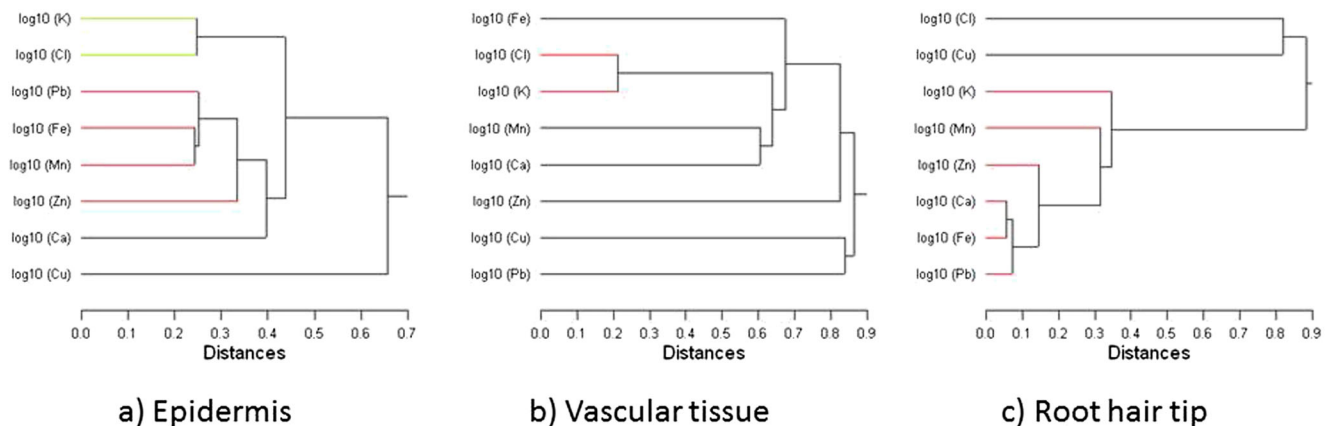


Fig. 7 a–c Results of the cluster analysis performed on the root epidermis, vascular tissue, and hair tip, respectively (linkage: single linkage method (nearest neighbor); distance: Pearson correlation coefficient)

addition, root hair cells secrete acid (H^+) that solubilizes the minerals into ionic form, making the ions to be taken up easily (MacFarlane and Burchett 2002; Lasat 2002; Verbruggen et al. 2009). Therefore, plant root hair can actively uptake metals and other elements from sediments and transport the nutrients in solution through the root xylem to the rest of plant tissue for growth. In some cases, the root hair is even capable of absorbing inorganic nutrients in solution against concentration gradient (Enstone et al. 2003).

Several early studies discussed the function of Fe plaque in metal transport in plant root system (e.g., St-Cyr and Campbell 1996; Sundby et al. 1998; Ye et al. 1998; Liu et al. 2004). Because of the high adsorption capacity of Fe oxides or Fe plaque, which is embedded in wetland plant roots, it is considered as a reactive substrate for metal sequestration (Deng et al. 2010; Hansel et al. 2001, 2002; Morrissey and Guerinet 2009; St-Cyr and Crowder 1990; Otte et al. 1989, 1991; Taylor et al. 1984). This study shows that other trace metals (e.g., Cu, Mn, Pb, and Zn) besides Fe were also found in the epidermis (Fig. 4). The results suggest that these trace metals may be combined with Fe plaque or Fe oxides and included in the high-attenuation substances as shown in Fig. 3 due possibly to scavenge by Fe plaque. Although synchrotron CMT measurement in this study cannot identify the chemical composition of the high-attenuation substances (Fig. 3), the information from synchrotron XRF measurement suggests that Fe must be included in this high-attenuation substance (Fig. 4). The presence of Fe plaque in the epidermis is further confirmed by synchrotron XANES measurement by setting the energy below and above Fe edge (Fig. 5). Because Fe has a relatively higher concentration than other trace metals (Fig. 4, Table 1), Fe should have a relatively higher attenuation than the other elements. It is reasonable to believe that this is Fe plaque that is predominantly Fe oxides (St-Cyr and Campbell 1996; Hansel et al. 2001). In other words, due to the formation of Fe plaque, Fe shows a relatively high concentration in the epidermis (Fig. 4, Table 1). The accumulation of Cu, Fe, Mn, Pb, and Zn in the epidermis and the significant correlation between trace metals (Cu, Mn, Pb, and Zn) and Fe (Fig. 6, $p < 0.001$) suggest that these trace elements were taken up by the plants and could be scavenged by Fe plaque in the epidermis (Fig. 6). In other words, high concentrations of Cu, Mn, Pb, and Zn in the epidermis can be adsorbed by Fe plaque or Fe-Mn oxides due to the large-specific surface area of iron oxides (which is often greater than $200 \text{ m}^2 \text{ g}^{-1}$) for metal sequestration (Hansel et al. 2001). Therefore, Fe plaque can provide a reactive substrate to scavenge metals (Bargar et al. 1997; Eick et al. 1999). High concentrations of Ca, Cl, Cu, and K as well as Mn and Zn in the vascular tissue can be a result of transportation of these metals by their individual transport protein, as suggested by factor analysis and cluster analysis (Table 2, Fig. 7).

Conclusion

This micro-scale investigation depicted metal concentrations and distributions in the *S. alterniflora* root system. The synchrotron XRF measurement showed that the average concentrations of Cl, Fe, Mn, Pb, and Zn in the epidermis were generally higher than those in the vascular tissue, while the average concentration of Ca in the epidermis was lower than that in the vascular tissue. The average concentrations of Cu and K in the epidermis and vascular tissue were comparable. Fe plaque was found in the root epidermis, where Cu, Mn, Pb, and Zn showed significant ($p < 0.001$) correlations with Fe possibly as a consequence of metal adsorption by Fe plaque. Although the role of Fe plaque in controlling metal biogeochemical cycle needs further study, the results have shown that the root epidermis can be an important environment to form Fe plaque and control metal uptake and transport by forming less mobile metal species and metal complexes. As a basic scientific research, the results from this study provide useful information on metal transportation and distribution in the *S. alterniflora* root system.

Acknowledgments This work was supported in part by the State Key Laboratory of Estuarine and Coastal Research Open Research Fund (Ref #: SKLEC-KF201304) (HF, WZ, LY, WL, YQ), the China Scholarship Council (YQ), and the Margaret and Herman Sokol Foundation (HF). This project was also supported in part by the U.S. Department of Energy, Office of Science, Office of Workforce Development for Teachers and Scientists (WDTS) under the Visiting Faculty Program (VFP) (HF). Use of the NSLS was supported by the U.S. Department of Energy, Office of Science, Office of Basic Energy Sciences, under Contract No. DE-AC02-98CH10886. NSLS X27A was supported in part by the U.S. Department of Energy - Geosciences (DE-FG02-92ER14244 to The University of Chicago - CARS). We are also grateful to Professor Elena Maestri, Editor of Environmental Science and Pollution Research, and the two anonymous reviewers who offered constructive comments and suggestions on an earlier draft of this paper.

Conflict of interest The authors declare that they have no competing interests.

Ethical statement The manuscript submitted to ESRP has not been submitted to more than one journal for simultaneous consideration. The manuscript is based on our original work and has not been published previously. No data in this manuscript were fabricated or manipulated (including images) to support the conclusions. All the references were properly cited to acknowledge other work. Consent to submit this manuscript has been received explicitly from all co-authors. Authors whose names appear on the submission have contributed sufficiently to the scientific work and therefore share collective responsibility and accountability for the results. The research did not involve any human participants and/or animals.

References

- Ablett JM, Kao CC, Reeder RJ, Tang Y, Lanzirotti A (2006) X27A—a new hard X-ray micro-spectroscopy facility at the National

- Synchrotron Light Source. Nucl Inst Methods Phys Res A 562:487–494
- Bargar JR, Brown GE, Parks GA (1997) Surface complexation of Pb(II) at oxide-water interface: II. XAFS and bond-valence determination of mononuclear Pb(II) sorption products and surface functional groups on iron oxides. *Geochim Cosmochim Acta* 61:2639–2652
- Chen XQ (1998) Changjiang (Yangtze) River Delta, China. *J Coast Res* 14:838–858
- Chen JY, Cheng HQ, Dai ZJ (2007) Compatibility of utilization and protection of tidal flat and wetland: a case study in Shanghai area. *China Eng Sci* 9:11–17 (in Chinese with English abstract)
- Cheng S (2003) Heavy metals in plants and phytoremediation. *Environ Sci Pollut Res* 10:335–340
- Dai WM, Gu YZ (1990) Accumulation of heavy metal elements in the sediments near Xiqu and Nanqu sewage outlets, Shanghai. *Shanghai Environ Sci* 9:38–40 (in Chinese)
- Deng D, Wu S-C, Wu F-Y, Deng H, Wong M-H (2010) Effects of root anatomy and Fe plaque on arsenic uptake by rice seedlings grown in solution culture. *Environ Pollut* 158:2589–2595
- Eick MJ, Peak JE, Brady PV, Pesek JD (1999) Kinetics of lead adsorption and desorption on goethite: residence time effect. *Soil Sci* 164:28–39
- Emerson D, Weiss JV, Megonigal JP (1999) Iron-oxidizing bacteria are associated with ferric hydroxide precipitates (Fe-plaque) on the roots of wetland plants. *Appl Environ Microbiol* 65:2758–2761
- Enstone DE, Peterson CA, Ma F (2003) Root endodermis and exodermis: structure, function, and responses to the environment. *J Plant Growth Regul* 21:335–351
- Feng H, Cochran JK, Lwiza H, Brownawell B, Hirschberg DJ (1998) Distribution of heavy metal and PCB contaminants in the sediments of an urban estuary: the Hudson River. *Mar Environ Res* 45:69–88
- Feng H, Han X, Zhang W, Yu L (2004) A preliminary study of heavy metal contamination in Yangtze River intertidal zone due to urbanization. *Mar Pollut Bull* 49:910–915
- Feng H, Qian Y, Gallagher FJ, Wu M, Zhang W, Yu L, Zhu Q, Zhang K, Liu C-J, Tappero R (2013) Lead accumulation and association with Fe on *Typha latifolia* root from an urban brownfield site. *Environ Sci Pollut Res* 20:3743–3750
- Frenzel P, Bosse U, Janssen PH (1999) Rice roots and methanogenesis in a paddy soil: ferric iron as an alternative electron acceptor in the rooted soil. *Soil Biol Biochem* 31:421–430
- Gilbert B, Frenzel P (1998) Rice roots and CH₄ oxidation: the activity of bacteria, their distribution and the microenvironment. *Soil Biol Biochem* 30:1903–1916
- Gleason SM, Ewel KC, Hue N (2003) Soil redox conditions and plant-soil relationships in a micronesia mangrove forest. *Estuar Coast Shelf Sci* 56:1065–1074
- Gotelli NJ, Ellison AM (2004) A primer of ecological statistics, 1st edn. Sinauer Associates, Sunderland, p 492
- Hansel CM, Fendorf S, Sutton S, Newville M (2001) Characterization of Fe plaque and associated metals on the roots of mine-waste impacted aquatic plants. *Environ Sci Technol* 35:3863–3868
- Hansel CM, Laforce MJ, Fendorf S, Sutton S (2002) Spatial and temporal association of As and Fe species on aquatic plant roots. *Environ Sci Technol* 36:1988–1994
- Hinsinger P, Courchesne F (2008) Biogeochemistry of metals and metalloids at the soil-root interface. In: Violante A, 404 *Plant Soil* (2009) 321,385–408
- Jones KW, Feng H (2002) Microanalysis of materials using synchrotron radiation. In: Sham TK (ed) Chemical applications of synchrotron radiation. World Scientific Publishing Company, New Jersey, pp 1010–1054
- Jones K, Feng H, Lanzirotti A, Mahajan D (2005) Synchrotron X-ray microprobe and computed microtomography for characterization of nanocatalysts. *Nucl Inst Methods Phys Res B Beam Interact Mater Atoms* 241:331–334
- Jones KW, Wang J, Chen Y, Yuan Q, Lindquist WB, Beckingham L, Peters CA, Um W, Newman L, Sabo-Attwood T, Tappero R (2013) Tomographic investigations relevant to the rhizosphere In: Anderson SH, Hopmans JW (eds) Soil-water-root processes: advances in tomography and imaging. SSSA special publication 61. Madison, Wisconsin, pp 23–39
- King GM, Garey MA (1999) Ferric iron reduction by bacteria associated with the roots of freshwater and marine macrophytes. *Appl Environ Microbiol* 65:4393–4398
- Koelmel J, Amarasiriwardena D (2012) Imaging of metal bioaccumulation in Hay-scented fern (*Dennstaedtia punctilobula*) rhizomes growing on contaminated soils by laser ablation ICP-MS. *Environ Pollut* 168:62–70
- Lacerda LD, Freixo JL, Coelho SM (1997) The effect of *Spartina alterniflora* Loisel on trace metals accumulation in inter-tidal sediments. *Mangrove Salt Marshes* 1:201–209
- Lasat MM (2002) Phytoextraction of toxic metals: a review of biological mechanisms. *J Environ Qual* 31:109–120
- Liu W-J, Zhu Y-G, Smith FA, Smith SE (2004) Do iron plaque and genotypes affect arsenate uptake and translocation by rice seedlings (*Oryza sativa* L.) grown in solution culture? *J Exp Bot* 55:1707–1713
- Liu M, Hou LJ, Xu SY, Ou DN, Yang Y, Yu J, Wang Q (2006) Organic carbon and nitrogen stable isotopes in the intertidal sediments from the Yangtze Estuary, China. *Mar Pollut Bull* 52:1625–1633
- Loring DH (1991) Normalization of heavy-metal data from estuarine and coastal sediments. *ICES J Mar Sci* 48:101–115
- Lyubanova L, Pongrac P, Vogel-Mikuš K, Mezek GK, Vavpetič P, Grlj N, Regvar M, Pelicon P, Schröder P (2013) The fate of arsenic, cadmium and lead in *Typha latifolia*: a case study on the applicability of micro-PIXE in plant ionomics. *J Hazard Mater* 248:371–378
- MacFarlane GR, Burchett MD (2002) Toxicity, growth and accumulation relationships of copper, lead and zinc in the grey mangrove, *Avicennia marina* (Forsk.) Vierh. *Mar Environ Res* 54:65–84
- Marques APGC, Rangel AOSS, Castro PML (2009) Remediation of heavy metal contaminated soils: phytoremediation as a potentially promising clean-up technology. *Crit Rev Environ Sci Technol* 39: 622–654
- Martin R, Naftel S, Macfie S, Jones K, Feng H, Trembley C (2006) High variability of the metal content of tree growth rings as measured by synchrotron micro x-ray fluorescence spectrometry. *X-Ray Spectrom* 35:57–62
- McLaughlin MJ, Smolders E, Merckx R (1998) Soil-root interface: physicochemical processes. In: Huang PM, Adriano DC, Logan TJ, Checkai RT (eds) Soil chemistry and ecosystem health. Soil Science Society of America, Madison, pp 233–277, **Special Publication no. 52**
- Morrissey J, Guerinot M (2009) Iron uptake and transport in plants: the good, the bad, and the ionome. *Chem Rev* 109:4553–4567
- Otte ML, Rozema J, Koster L, Haarsma MS, Broekman RA (1989) Iron plaque on roots of *Aster tripolium* L.: interaction with zinc uptake. *New Phytol* 111:309–317
- Otte ML, Dekkers MJ, Rozema J, Broekman RA (1991) Uptake of arsenic by *Aster tripolium* in relation to rhizosphere oxidation. *Can J Bot* 69:2670–2677
- Perret D, Gaillard J, Dominik J, Attea O (2000) The diversity of natural hydrous iron oxides. *Environ Sci Technol* 34:3540–3546
- Punshon T, Guerinot M, Lanzirotti A (2009) Using synchrotron X-ray fluorescence microprobes in the study of metal homeostasis in plants. *Ann Bot* 103:665–672
- Qian Y, Gallagher FJ, Feng H, Wu M (2012) A geochemical study of toxic metal translocation in an urban brownfield wetland. *Environ Pollut* 166:23–30
- Rotkittikhum P, Kruatrachue M, Chaiyarat R, Ngernsarsaruy C, Pokethitiyook P, Pajitprapaporn A, Baker AJM (2006) Uptake

- and accumulation of lead by plants from the Bo Ngam lead mine area in Thailand. *Environ Pollut* 144:681–688
- St-Cyr L, Campbell PGC (1996) Metals (Fe, Mn, Zn) in the root plaque of submerged aquatic plants collected in situ: relations with metal concentrations in the adjacent sediments and in the root tissue. *Biogeochemistry* 33:45–76
- St-Cyr L, Crowder AA (1990) Manganese and copper in the root plaque of *Phragmites australis* (Cav.) Trin. ex Steudel. *Soil Sci* 149:191–198
- Sundby B, Vale C, Caçador I, Catarino F, Madureira MJ, Caetano M (1998) Metal-rich concretions on the roots of salt marsh plants: mechanism and rate of formation. *Limnol Oceanogr* 43:245–252
- Sutton SR, Bertsch PM, Newville M, Rivers ML, Lanzirotti A, Eng PJ (2002) Microfluorescence and microtomography analyses of heterogeneous earth and environmental materials. In: Fenter PA, Rivers ML, Sturchio NC, Sutton SR (eds) *Applications of synchrotron radiation in low-temperature geochemistry and environmental science*, vol 49. Mineralogical Society of America, Chantilly, pp 429–483
- Tangahu BV, Abdullah SRS, Basri H, Idris M, Anuar N, Mukhlisin M (2011) A review on heavy metals (As, Pb, and Hg) uptake by plants through phytoremediation. *Int J Chem Eng* 1–31. doi:10.1155/2011/939161
- Taylor SR, McLennan SM (1995) The geochemical evolution of the continental crust. *Rev Geophys* 33:241–265
- Taylor GJ, Crowder AA, Rodden R (1984) Formation and morphology of an iron plaque on the roots of *Typha latifolia* L. grown in solution culture. *Am J Bot* 71:666–675
- Tripathi RD, Tripathi P, Dwivedi S, Kumar A, Mishra A, Chauhan PS, Norton GJ, Nautiyal CS (2014) Roles for root iron plaque in sequestration and uptake of heavy metals and metalloids in aquatic and wetland plants. *Metallomics* 6:1789–1800
- Verbruggen N, Hermans C, Schat H (2009) Molecular mechanisms of metal hyperaccumulation in plants. *New Phytol* 181:759–776
- Wang TG, Pevery JH (1999) Iron oxidation states on root surfaces of a wetland plant (*Phragmites australis*). *Soil Sci Soc Am J* 63:247–252
- Wang J, Chen YK, Yuan Q, Tkachuk A, Erdonmez C, Hornberger B, Feser M (2012) Automated markerless full field hard x-ray microscopic tomography at sub-50 nm 3-dimension spatial resolution. *Appl Phys Lett* 100:143–107
- Wang J, Chen-Wiegart YK, Wang J (2013) *In situ* chemical mapping of a lithium-ion battery using full-field hard X-ray spectroscopic imaging. *Chem Commun* 49:6480–6482
- Wang J, Chen-Wiegart YK, Wang J (2014a) *In situ* three-dimensional synchrotron X-ray nanotomography of the (de)lithiation processes in tin anodes. *Angew Chem Int Ed* 53(17):4460–4464
- Wang J, Chen-Wiegart YK, Wang J (2014b) *In operando* tracking phase transformation evolution of lithium iron phosphate with hard X-ray microscopy. *Nat Commun*, 5. doi: 10.1038/ncomms5570
- Weis JS, Weis P (2004) Metal uptake, transport and release by wetland plants: implications for phytoremediation and restoration. *Environ Int* 30:685–700
- Williams TP, Bubbs JM, Lester JN (1994) Metal accumulation within salt marsh environments: a review. *Mar Pollut Bull* 28:273–290
- Windham L, Weis JS, Weis P (2003) Uptake and distribution of metals in two dominant salt marsh macrophytes, *Spartina alterniflora* (cordgrass) and *Phragmites australis* (common reed). *Estuar Coast Shelf Sci* 56:63–72
- Wu H, Zhu JR, Choi BH (2010) Links between saltwater intrusion and subtidal circulation in the Changjiang estuary: a model-guided study. *Cont Shelf Res* 30:1891–1895
- Ye ZH, Baker AJM, Wong MH, Willis AJ (1998) Zinc, lead and cadmium accumulation and tolerance in *Typha latifolia* as affected by iron plaque on the root surface. *Aquat Bot* 61:55–67
- Zhang W, Yu L, Hutchinson SM, Xu S, Chen Z, Gao X (2001) China's Yangtze estuary: I. Geomorphic influence on heavy metal accumulation in intertidal sediments. *Geomorphology* 41:195–205
- Zhang W, Feng H, Chang J, Qu J, Xie H, Yu L (2009) Heavy metal contamination in surface sediments of Yangtze River intertidal zone: an assessment from different indexes. *Environ Pollut* 157:1533–1543